Skyrmion oscillations in magnetic nanorods with chiral interactions

M. Charilaou* and J. F. Löffler

Laboratory of Metal Physics and Technology, Department of Materials, ETH Zurich, 8093 Zurich, Switzerland

(Received 15 November 2016; published 10 January 2017)

We report that in cylindrical nanorods with chiral interactions spin textures corresponding to spatial skyrmion oscillations can be stabilized depending on the initial state, as revealed by micromagnetic calculations. The skyrmion oscillation, or skyrmion-chain state, occurs when the diameter of the rod is larger than the helical pitch length of the material, and the number of skyrmions on the chain is proportional to the length of the nanorod. The topological charge is localized, breaking translational symmetry, but in the presence of a uniaxial anisotropy, or upon the application of an external field, the localization disappears and a single skyrmion line is formed. These findings provide a deeper understanding of the interplay between geometry and topology, and show how spatial confinement specifically in curved solids can stabilize skyrmionic spin textures.

DOI: 10.1103/PhysRevB.95.024409

I. INTRODUCTION

Competition between the symmetric exchange interaction and the antisymmetric Dzyaloshinskii-Moriya interaction (DMI) [1] can give rise to the formation of complex spin textures in magnetic matter. A fascinating example is the occurrence of skyrmions [2–7] and skyrmion lattices [8–11] upon the application of an external field or in the presence of uniaxial anisotropy. Magnetic skyrmions are topological particlelike spin configurations that are characterized by an integer topological charge (winding number as defined for spin textures) [12]

$$Q = \frac{1}{4\pi}\int \mathbf{m}\cdot(\partial_x\mathbf{m}\times\partial_y\mathbf{m})dxdy, \tag{1}$$

which can be either 1 (skyrmion) or -1 (antiskyrmion), where $\mathbf{m}$ is the unit vector of the magnetization ($\mathbf{m} = \mathbf{M}/M_S$ with M_S the saturation magnetization).

The intense research on skyrmions is fueled on the one hand by the new fundamental physics related to these complex spin structures, and on the other hand by the potential to develop new technology for data-storage devices. The latter is motivated by the fact that skyrmions can be moved by relatively low current densities [13–17], promising energy-efficient spintronics, and the compatibility of skyrmion-based devices with domain-wall-based technology, which can be achieved by adjusting the geometry of the solid [18].

In bulk crystals with free surfaces skyrmions exist in a narrow temperature-field range, close to the Curie temperature [8,19,20], but in thin films the skyrmion phase extends to wider temperature and field ranges [7,20], and in nanostructured materials skyrmions are stable even at room temperature [21,22]. The stability of skyrmionic states is crucially dependent on the low dimensionality and symmetry of the solid, as it confines the spin structure [23–25]. The confinement of skyrmionic spin textures in nanostructures is thus a key element in creating and controlling them. As we will discuss in the following, using high-resolution micromagnetic simulations considering B20 FeGe, the geometry of cylindrical nanostructures can give rise to nontrivial spin textures, which break translational symmetry in the form of spatially oscillating topological charge.

II. THEORETICAL MODEL

For the theoretical description of magnetism in FeGe nanorods we consider the following contributions to the total free energy density F: (i) ferromagnetic exchange

$$F_{\text{exc}} = A_{\text{exc}}(\nabla\mathbf{m})^2, \tag{2}$$

where A_{exc} is the exchange stiffness; (ii) Dzyaloshinskii-Moriya interaction

$$F_{\text{DMI}} = D\mathbf{m}\cdot(\nabla\times\mathbf{m}), \tag{3}$$

where D is the strength of the DMI; (iii) Zeeman energy

$$F_{\text{Z}} = -\mu_0 M_S \mathbf{H}_{\text{ext}}\cdot\mathbf{m}, \tag{4}$$

where $\mathbf{H}_{\text{ext}}$ is the external field; and (iv) magnetostatic self-energy due to dipolar interactions

$$F_{\text{dip}} = -\frac{\mu_0 M_S}{2}\mathbf{m}\cdot\mathbf{h}_{\text{demag}}, \tag{5}$$

where $\mathbf{h}_{\text{demag}}$ is the local demagnetizing field.

We start the simulations at a fully polarized configuration (energy maximum), and observe the evolution of the spin texture inside the solid as a function of time by solving the Landau-Lifshitz-Gilbert equation of motion

$$\partial_t\mathbf{m} = -\mu_0\gamma(\mathbf{m}\times\mathbf{h}_{\text{eff}}) + \alpha(\mathbf{m}\times\partial_t\mathbf{m}), \tag{6}$$

where α is the dimensionless damping parameter [$\alpha = G/(\gamma M_S)$], with G the Gilbert damping frequency constant and γ the electron gyromagnetic ratio, and $\mathbf{h}_{\text{eff}} = -[1/(\mu_0 M_S)]\partial_{\mathbf{m}}F$ is the effective magnetic field consisting of both internal and external fields. The material parameters for FeGe taken from literature are: exchange stiffness $A_{\text{exc}} = 8.78$ pJ/m [26], saturation magnetization $M_S = 385$ kA/m [27,28], and DMI strength $D = 1.58$ mJ/m^2 [26]. Since the DMI energy in FeGe is intrinsic and not of interfacial origin, it should not depend on the thickness, hence the DMI strength was kept constant throughout this study. For the numerical calculations the graphics-processing-unit accelerated software package *MuMax3* [29] was used in the high-damping case with $\alpha = 0.1$ (occasional checks with $\alpha = 0.01$ were made to test

*charilaou@mat.ethz.ch

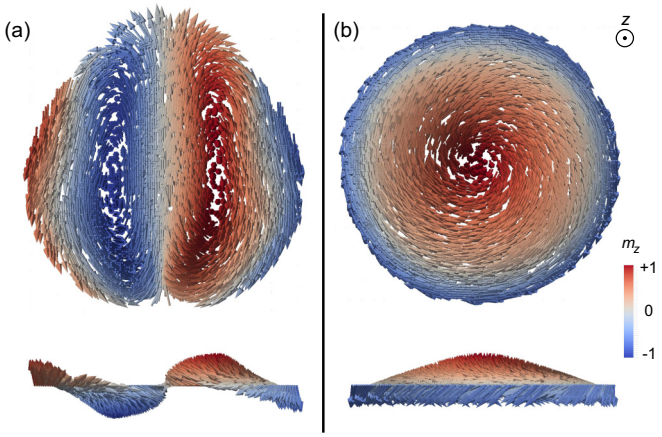

FIG. 1. Simulated ultrathin nanodisks with diameter of 120 nm after an external field of 1 T has been applied (a) in-plane and (b) out-of-plane. In (b) a skyrmion core forms.

the effects of damping on the simulation findings). Simulations were performed with different cell sizes to test the numerical stability, with the smallest cell tested being 1 nm^3. Even though very small sizes were used, quantum-mechanical effects were not considered in our simulations.

III. RESULTS AND DISCUSSION

We begin the discussion by considering ultrathin FeGe nanodisks. A crucial aspect for the realization of a skyrmion in an ultrathin structure is the presence of a perpendicular symmetry-breaking field, either external or internal, e.g., perpendicular magnetic anisotropy (PMA). Without an external field or PMA, the state with lowest energy corresponds to a helical spin texture [see Fig. 1(a)]. If, however, we prepare the skyrmion state by magnetizing the sample in the out-of-plane direction using an external field ($\mu_0 H_z = 1$ T) and then switching off the field, the resulting spin texture is that of a left-handed skyrmion core [see Fig. 1(b)], in which the z component of the magnetization in the center of the disk is $m_z = +1$ and at the edge of the disk it is $m_z \approx -1$. The numerical value of the topological charge for this spin texture is $Q \approx 0.85$ (for a perfect skyrmion of $Q = \pm 1$). The deviation from the integer value is due to the tilting of the spins along the circumference of the disk by dipolar interactions [23,26], which generally tend to align the moments along the physical edge of the solid [30]. A similar scenario, i.e., where the skyrmion state can be prepared by a sequence of magnetic fields, was experimentally observed in artificial skyrmion lattices [31].

The formation of the skyrmion core, instead of the helical state, can be explained with topological arguments: in order to transfer from a collinear perpendicular state (global energy maximum) to a helical state (global energy minimum), the spin texture needs to undergo curling, which begins by a twisting of the spins near the edges of the disk. The twisting at the edges lowers the total energy because it favors both the dipole-dipole interaction and DMI energy, and the system is trapped in this state (local energy minimum) because there is no continuous way to transfer the spin texture to a helical state due to the confinement by the solid. In contrast, if the system is fully polarized in the plane, there is a direct way to transfer the spin texture from the collinear state to the helical state, thus generating the texture as seen in Fig. 1(a).

For the confinement of the skyrmionic spin texture, the diameter (d) of the disk needs to be comparable to the skyrmion-core diameter, which depends on the interplay between the DMI and magnetostatic interactions [23]. For $d > 135$ nm the spin texture forms concentric rings with alternating m_z (not shown), similar to those discussed in Refs. [23,26,32]. While the upper limit is set by the formation of the ring state, defining a lower limit for d is not straightforward, since with decreasing diameter the skyrmion core becomes increasingly incomplete, and for very small d it corresponds to a conical state. (This again shows that the transformation from a conical spin configuration to a skyrmion is continuous in a nanodisk.) We find, however, that a single skyrmion in FeGe ultrathin disks is stable for diameters in the range of 70 nm

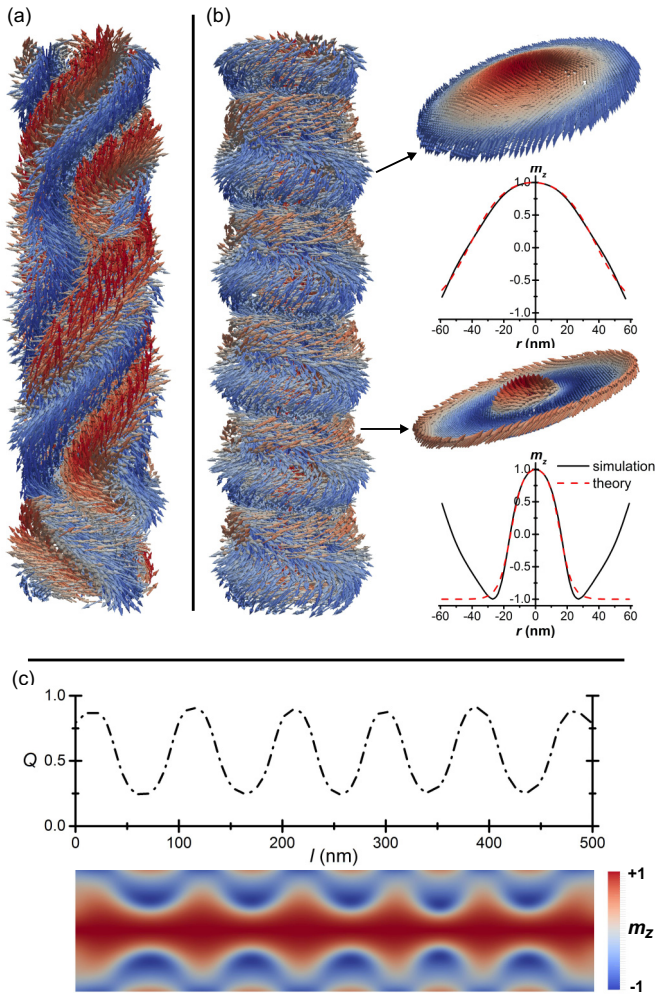

FIG. 2. Spin configurations in cylindrical nanowires with a length of 500 nm and a diameter of 120 nm showing (a) the helicoid state and (b) the skyrmion state with oscillating spin texture. The two slices and their respective magnetization profile show the two modes of oscillation. The dashed line is a fit with the 2π domain wall profile (see text). (c) A contour plot of the z component of the magnetization inside the nanowire shown in (b) and the oscillation of the topological charge [see Eq. (1)] Q along the wire.

($Q = 0.7$) to 135 nm ($Q = 0.84$), i.e., $\lambda < d < 2\lambda$, where $\lambda = 4\pi A_{\rm exc}/D \approx 70$ nm is the characteristic pitch length for FeGe.

Note that without dipolar interactions the upper limit for a single skyrmion core is $d < 90$ nm. Hence, dipolar interactions are crucial in stabilizing the skyrmion, as they tend to align the spins along the physical edge of the disk, thus shrinking or stretching the skyrmion in order to satisfy this condition. This importance of dipolar interactions was recently discussed with regards to experiments on Pt/Co/MgO nanostructures [22]. The interplay between dipolar interactions and DMI can be studied by the two characteristic lengths, i.e., λ and the exchange length [12,33] $\delta_M = 2\sqrt{A_{\rm exc}/(\mu_0 M_S^2)}$, which for FeGe is 14 nm. When $\lambda >> \delta_M$, the curling period of the spin structure is longer than the exchange length. As, however, the DMI increases and λ decreases, the curling is impeded by the dipolar interactions and the role of magnetostatics becomes more important.

Now we turn to three-dimensional (3D) structures, cylindrical nanowires, in order to examine the dimensional evolution of the skyrmion state in cylindrical geometry. The state was prepared in the same way as for the nanodisks, i.e., initializing the system at an energy maximum and observing the resulting state. Similar to the nanodisks, there are two competing states: the helicoid (distorted helical) [34] state and the skyrmion state. The helicoid state, prepared by applying an external field perpendicular to the rod axis, is shown in Fig. 2(a) for a nanorod with 120 nm diameter and 500 nm length. If we apply the external field along the rod axis, however, the resulting spin structure is a striking spin texture with broken translational symmetry, where the core of the rod is magnetized along the z axis and the outer regions are magnetized in the opposite directions, with a distinct spatial oscillation [see Fig. 2(b)]. The oscillation of the spin structure is characterized by the oscillation of the topological charge Q, as shown in Fig. 2(c), which oscillates between $Q \approx 0.9$ and $Q \approx 0.2$ with a sinusoidal form $Q \propto \sin(\pi l/\Lambda)$, with a period of $\Lambda = 95$ nm. The regions with high Q correspond to skyrmion formations, whereas the low Q regions resemble a ring formation [23,26,32], a mexican-hat-like spin texture.

Figure 2(b) shows slices of the spin structure in these two regions, and the corresponding magnetization profile. The core profile of both regions can be fitted well by that of a 2π domain, i.e., the profile of a skyrmion, which has the form [12] $\theta_{\rm m} = \theta_{\rm s}(-r/\delta_{\rm s} + R) + \theta_{\rm s}(-r/\delta_{\rm s} - R)$, with $\theta_{\rm s}(\xi) = 2\arctan e^{\xi}$, where θ_m is the angle of the magnetic moment at the distance r away from the center (here the distance from the wire center), R is a variational parameter, and $\delta_{\rm s}$ is the skyrmion radius. Hence, both regions contain a skyrmion core, but in the low Q region the spin texture at the edge has an opposite winding nearly canceling that of the inner skyrmion core, thus reducing Q. Given that the translational symmetry is broken, and despite the fact that the spin texture appears continuous, the state seen in Fig. 2(b) corresponds to a *skyrmion chain*, or a skyrmion stack, since the skyrmions are stacked/displaced vertically from each other.

In order to find the rod diameters, for which the skyrmion-chain state is stable, we have simulated conical structures, with a base diameter of 200 nm and a tip diameter of 25 nm, having an inclination of 2.5° over a length of 4 μm. Figure 3 shows a vector plot of the spin texture and a contour plot of the magnetization along the z axis of the cone. On going from a very thin nanowire to a 200 nm thick nanowire we find a number of possible states: for small diameters ($d \leqslant 60$ nm) we obtain a nearly

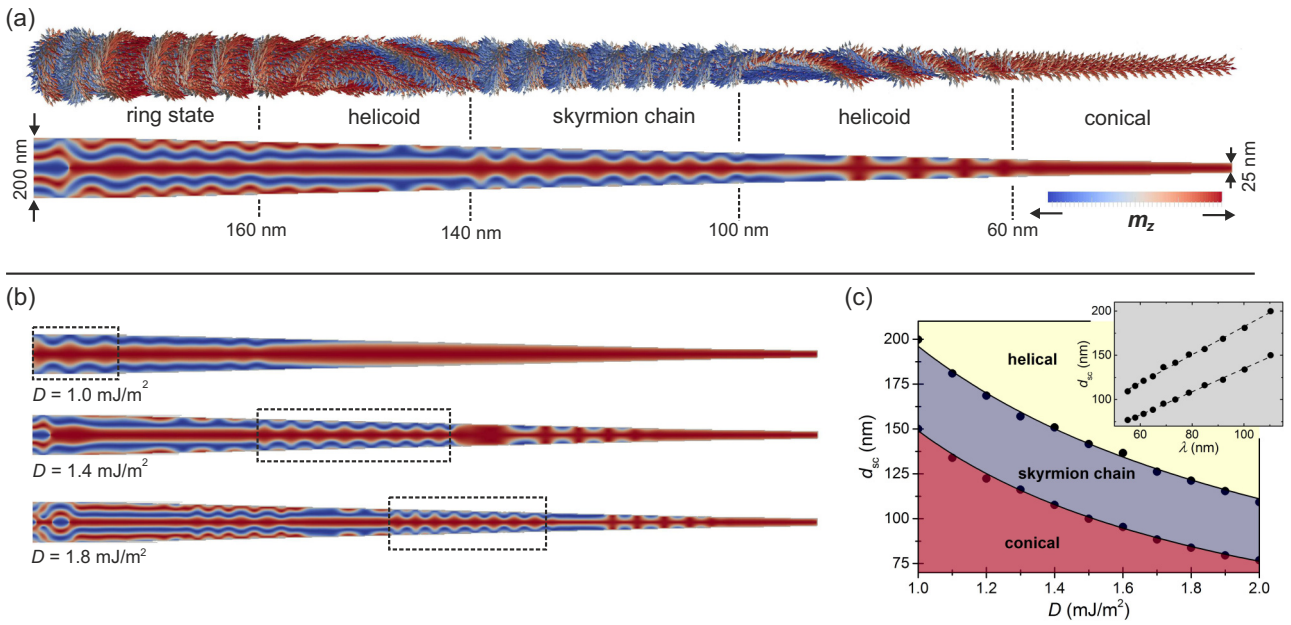

FIG. 3. (a) Snapshot of simulation performed on a FeGe cone, showing the possible spin textures at each range of diameters, starting with a conical spin structure for thin rods $d \leqslant 60$ nm, then a helicoid spin structure for $60 < d \leqslant 100$ nm, entering the skyrmion-chain state for $100 < d \leqslant 140$ nm, then again a helicoid structure for $140 < d \leqslant 160$ nm, which then transforms to a ring state for $d > 160$ nm. (b) Comparison between three systems with different DMI strength and (c) diameter ($d_{\rm sc}$) at which the skyrmion-chain state becomes stable as a function of DMI strength; circles are simulation results and solid lines are fits using $d_{\rm sc} \propto 1/D$: $d_{\rm sc}$ is proportional to the characteristic pitch length [inset to (c)].

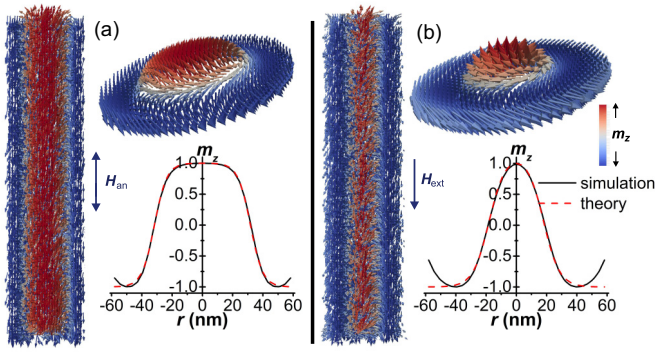

FIG. 4. Cross section of cylindrical nanowires with diameter 120 nm and length 500 nm with (a) a uniaxial anisotropy (K_u), and (b) an external field. The spin structure corresponds to that of a single skyrmion line, characterized by the absence of oscillations in Q. The dashed line is a fit with the 2π domain wall profile.

collinear texture with some curling on the edge of the solid, corresponding to a conical state; for $60 \leqslant d \leqslant 100$ nm we find a helicoid structure, which is the 3D analog of the 2D helical structure in Fig. 1(a); then, for $100 \leqslant d \leqslant 140$ nm we find the skyrmion-chain state, as shown in Fig. 2(b). For $d > 140$ nm a helicoid texture is favored, which transforms to a complex ring-state oscillation that unfolds via the formation of hedgehogs, or Bloch points, similar to those shown by Milde *et al.* [35].

In order to find the stability range of the skyrmion-chain state, we have simulated nanowires with different DMI strength and diameter, and we find that the diameters (d_{sc}) for which the skyrmion-chain state is stable are proportional to the characteristic length $d_{sc} \propto \lambda \propto 1/D$, i.e., when the DMI is increased (λ is decreased) the skyrmion-chain state is stable in thinner nanorods, and vice versa [see Fig. 3(c)]. This shows how these complex spin textures are the result of competition between the different energy contributions (exchange and DMI) and their characteristic lengths.

In the skyrmion-chain state the localization of Q can be suppressed by adding anisotropy in the energy of the system, either with an external field or with uniaxial anisotropy. Let us consider a hypothetical scenario of a system with exactly the same material parameters (M_S, A_{exc}, and D) as FeGe, which additionally has a uniaxial magnetocrystalline anisotropy K_u (see Fig. 4). For very small anisotropy ($K_u < 10^3$ J/m^3) the skyrmion oscillation remains unchanged, but with increasing K_u, the oscillation of Q in the nanowire gradually decreases (we quantify this by measuring $\Delta Q = Q_{max} - Q_{min}$), and for $K_u > 2 \times 10^4$ J/m^3 the oscillation vanishes. Figure 4(a) shows the spin structure for $K_u = 10^5$ J/m^3 (we chose this value because it is comparable to the magnetostatic self-energy $\mu_0 M_S^2/2$), which is a continuous *skyrmion line* along the rod with $Q = 0.85$.

Similarly, if we break the symmetry by an external field along the z direction opposing the magnetization in the core (without having K_u), the resulting spin configuration is again a single skyrmion line along the rod [see Fig. 4(b)]. For a one-to-one comparison between the effect of internal vs external field, the applied field in this example was set equal to the anisotropy field from the example shown in Fig. 4(a), i.e., ($|\mu_0 H_z| = \mu_0 H_{an} = 2K_u/M_S = 0.52$ T). The external field not only generates a single skyrmion line, but also decreases the skyrmion radius. In fact, with increasing (opposing) H_z, the skyrmion radius decreases monotonically up to the critical field, at which $Q \to 0$ and $m_z \to -1$. Once $m_z = -1$, if we switch off the external field, the spin configuration will return to that of a skyrmion chain, but with opposite polarity. When the external field is applied parallel to the polarity in the rod, the skyrmion radius dramatically decreases and vanishes for very small fields (in this case 100 mT).

All the predictions made here may be verified experimentally, either by real-space observation, i.e., Lorentz transmission electron microscopy or magnetic force microscopy, or by reciprocal space investigations, such as polarized small-angle neutron scattering. It is expected that the material properties might deviate from the values used in this study, due to inhomogeneities, roughness, and the free surfaces, and this could have an effect on the nanowire diameters, for which the described magnetic state can be observed, as these are proportional to the characteristic length λ.

IV. CONCLUSIONS

In summary, we have shown that geometrical confinement in cylindrical nanowires enables the occurrence of nontrivial skyrmion chains with broken translational symmetry, with a distinct oscillation of the topological charge along the wire. The wire thicknesses, for which this state is stable, depend linearly on the characteristic helical pitch-length of the material, which in turn depends on the ratio between the strength of the ferromagnetic exchange stiffness and the Dzyaloshinskii-Moriya interaction. An external field or uniaxial anisotropy can turn the structure to that of a single skyrmion line, restoring translational symmetry. These findings provide a deeper understanding of the stability of skyrmionic spin configurations in nanostructures, where spatial confinement plays a vital role. They may also be of great importance for the further development of spintronics towards skyrmion-based technologies, where cylindrical nanostructures can be used to inject/read skyrmions when coupled to other devices.

ACKNOWLEDGMENTS

We would like to thank H.-B. Braun and C. Moutafis for fruitful discussions. This work was funded by the ETH Zurich.

[1] I. E. Dzyaloshinskii, Sov. Phys. JETP **5**, 1259 (1957); T. Moriya, Phys. Rev. **120**, 91 (1960).
[2] T. H. A. Skyrme, Proc. R. Soc. London Ser. A **260**, 127 (1961).
[3] A. N. Bogdanov and D. A. Yablonskii, Sov. Phys. JETP **68**, 101 (1989).
[4] A. N. Bogdanov and U. K. Rössler, Phys. Rev. Lett. **87**, 037203 (2001).

[5] U. K. Rössler, A. N. Bogdanov, and C. Pfleiderer, Nature (London) **442**, 797 (2006).
[6] M. Bode, M. Heide, K. von Bergmann, P. Ferriani, S. Heinze, G. Bihlmayer, A. Kubetzka, O. Pietzsch, S. Blügel, and R. Wiesendanger, Nature (London) **447**, 190 (2007).
[7] S. X. Huang and C. L. Chien, Phys. Rev. Lett. **108**, 267201 (2012).
[8] X. Z. Yu, N. Kanazawa, Y. Onose, K. Kimoto, W. Z. Zhang, S. Ishiwata, Y. Matsui, and Y. Tokura, Nat. Mater. **10**, 106 (2010).
[9] S. Heinze, K. von Bergmann, M. Menzel, J. Brede, A. Kubetzka, R. Wiesendanger, G. Bihlmayer, and S. Blügel, Nat. Phys. **7**, 713 (2011).
[10] S. Buhrandt and L. Fritz, Phys. Rev. B **88**, 195137 (2013).
[11] X. Yu, J. P. DeGrave, Y. Hara, T. Hara, S. Jin, and Y. Tokura, Nano Lett. **13**, 3755 (2013).
[12] H. B. Braun, Adv. Phys. **61**, 1 (2012).
[13] F. Jonietz, S. Mühlbauer, C. Pfleiderer, A. Neubauer, W. Münzer, A. Bauer, T. Adams, R. Georgii, P. Böni, R. A. Duine, K. Everschor, M. Garst, and A. Rosch, Science **330**, 1648 (2010).
[14] J. Iwasaki, M. Mochizuki, and N. Nagaosa, Nat. Commun. **4**, 1463 (2013).
[15] A. Fert, V. Cros, and J. Sampaio, Nat. Nano. **8**, 152 (2013).
[16] J. Sampaio, V. Cros, S. Rohart, A. Thiaville, and A. Fert, Nat. Nano. **8**, 839 (2013).
[17] Y. Zhou, E. Iacocca, A. Awad, R. K. Dumas, F. C. Zhang, H. B. Braun, and J. Åkerman, Nat. Commun. **6**, 8193 (2015).
[18] Y. Zhou and M. Ezawa, Nat. Commun. **5**, 4652 (2014).
[19] S. Mühlbauer, B. Binz, F. Jonietz, C. Pfleiderer, A. Rosch, A. Neubauer, R. Georgii, and P. Böni, Science **323**, 915 (2009).
[20] X. Z. Yu, Y. Onose, N. Kanazawa, J. H. Park, J. H. Han, Y. Matsui, N. Nagaosa, and Y. Tokura, Nature (London) **465**, 901 (2010).
[21] C. Moreau-Luchaire, C. Moutafis, N. Reyren, J. Sampaio, C. A. F. Vaz, N. Van Horne, K. Bouzehouane, K. Garcia, C. Deranlot, P. Warnicke, P. Wohlhüter, J.-M. George, M. Weigand, J. Raabe, V. Cros, and A. Fert, Nat. Nano. **11**, 444 (2016).
[22] O. Boulle, J. Vogel, H. Yang, S. Pizzini, D. de Souza Chaves, A. Locatelli, T. O. Mentes, A. Sala, L. D. Buda-Prejbeanu, O. Klein, M. Belmeguenai, Y. Roussigné, A. Stashkevich, S. M. Chérif, L. Aballe, M. Foerster, M. Chshiev, S. Auffret, I. M. Miron, and G. Gaudin, Nat. Nano. **11**, 449 (2016).
[23] S. Rohart and A. Thiaville, Phys. Rev. B **88**, 184422 (2013).
[24] R. Streubel, P. Fischer, F. Kronast, V. P. Kravchuk, D. D. Sheka, Y. Gaididei, O. G. Schmidt, and D. Makarov, J. Phys. D: Appl. Phys. **49**, 363001 (2016).
[25] V. P. Kravchuk, U. K. Rössler, O. M. Volkov, D. D. Sheka, J. van den Brink, D. Makarov, H. Fuchs, H. Fangohr, and Y. Gaididei, Phys. Rev. B **94**, 144402 (2016).
[26] M. Beg, R. Carey, W. Wang, D. Cortés-Ortuño, M. Vousden, M.-A. Bisotti, M. Albert, D. Chernyshenko, O. Hovorka, R. L. Stamps, and H. Fangohr, Sci. Rep. **5**, 17137 (2015).
[27] T. Ericsson, W. Karner, L. Häggström, and K. Chandra, Phys. Scr. **23**, 1118 (1981).
[28] H. Yamada, K. Terao, H. Ohta, and E. Kulatov, Physica B **329-333**, 1131 (2003).
[29] A. Vansteenkiste, J. Leliaert, M. Dvornik, M. Helsen, F. Garcia-Sanchez, and B. Van Waeyenberge, AIP Adv. **4**, 107133 (2014).
[30] M. Charilaou and F. Hellman, J. Appl. Phys. **117**, 083907 (2015).
[31] D. A. Gilbert, B. B. Maranville, A. L. Balk, B. J. Kirby, P. Fischer, D. T. Pierce, J. Unguris, J. A. Borchers, and K. Liu, Nat. Commun. **6**, 8462 (2015).
[32] C. Moutafis, S. Komineas, C. A. F. Vaz, J. A. C. Bland, T. Shima, T. Seki, and K. Takanashi, Phys. Rev. B **76**, 104426 (2007).
[33] J. F. Löffler, H. B. Braun, and W. Wagner, Phys. Rev. Lett. **85**, 1990 (2000).
[34] A. B. Butenko, A. A. Leonov, U. K. Rössler, and A. N. Bogdanov, Phys. Rev. B **82**, 052403 (2010).
[35] P. Milde, D. Köhler, J. Seidel, L. M. Eng, A. Bauer, A. Chacon, J. Kindervater, S. Mühlbauer, C. Pfleiderer, S. Buhrandt, C. Schütte, and A. Rosch, Science **340**, 1076 (2013).